Reprinted from The Journal of Physical Chemistry, 1991, 95.

Molecular Dynamics Simulation of Electron Transfer in Proteins. Theory and Application to $Q_A \rightarrow Q_B$ Transfer in the Photosynthetic Reaction Center

M. Nonella and K. Schulten*

Beckman Institute and Department of Physics, University of Illinois, Urbana, Illinois 61801
(Received: October 2, 1990)

Electron transfer (ET) from the primary menaquinone Q_A to the secondary ubiquinone Q_B, i.e., $Q_A^-Q_B \rightarrow Q_AQ_B^-$, in the photosynthetic reaction center of *Rhodopseudomonas viridis* has been simulated by using the method of molecular dynamics accounting for the classical motion of a protein's nuclear degrees of freedom, the redistribution of charge accompanying electron transfer being described quantum chemically. We outline the role of classical nuclear degrees of freedom in electron transfer, identifying the essential dynamic properties that should be determined from molecular dynamics simulations in order to characterize electron transfer. These quantities, all related to the energy difference $\Delta E(t) = E_P(t) - E_R(t)$ of *virtual* forward (electron *tries* to jump forward before ET) and backward (electron *tries* to jump backward after ET) electron transfer, R and P denoting the states $Q_A^-Q_B$ and $Q_AQ_B^-$, respectively, are as follows: the variance of $\Delta E(t)$ and the average value of $\Delta E(t)$ before and after transfer, i.e., Σ_R (6.9 kcal/mol), $\langle \Delta E \rangle_R$ (22 kcal/mol) and Σ_P (8.8 kcal/mol), $\langle \Delta E \rangle_P$ (−25 kcal/mol), respectively; the relaxation time of the energy–energy correlation function $\langle (\Delta E(t) - \langle \Delta E \rangle_R)(\Delta E(0) - \langle \Delta E \rangle_R) \rangle_R$ (120 fs); the time describing the relaxation of $\Delta E(t)$ from an average value $\langle \Delta E \rangle_R$ to an average value $\langle \Delta E \rangle_P$ immediately after electron transfer (200 fs). The quantities in brackets are the respective simulation results. We determined also the free enthalpy difference of the transfer $Q_A^-Q_B \rightarrow Q_AQ_B^-$ (−3.4 kcal/mol). Our simulations indicate that the motion of the non-heme iron of the reaction center is not coupled to the $Q_A^-Q_B \rightarrow Q_AQ_B^-$ transfer. Interaction energies of Q_B in different charge states with the protein environment have been calculated and reflect a stronger binding of Q_B^- and Q_B^{2-} compared to that of Q_B.

1. Introduction

Photosynthesis is one of the most important and most widely studied processes in living systems. The primary steps in photosynthesis involve the absorption of light energy and its conversion into an electrochemical potential. In photosynthetic bacteria the step takes place in the so-called photosynthetic reaction center, a large protein-pigment complex, located in the cellular membrane. In the past such processes have been investigated in solvents, an area of inquiry that was very much influenced by the seminal work of Weller.[1] For a long time photoinduced electron transfer in solvents was much better understood than that in photosynthetic proteins due to the many systems available for study and due to the seemingly simpler and better defined environment in which the transfer takes place. However, the availability of high-resolution X-ray structures of the reaction centers of the purple bacteria *Rhodopseudomonas viridis* and *Rhodopseudomonas sphaeroides* recently determined[2,3] reversed the situation. Detailed reviews of the primary electron-transfer steps of photosynthesis can be found in refs 7–9.

In particular, the available structures allow one to explore the mechanism of light energy conversion in these systems using the method of molecular dynamics simulation. Such simulations are considered today an important source of information on protein structure, function, and mechanism.[4-6] These simulations can also provide an extremely detailed view of the electron-transfer process. Many questions addressed by the pioneers of photoinduced electron transfer in solution can now be answered, and details concerning the coupling between charge displacement and solvent motion can be uncovered.

The reaction center complex of *Rhodopseudomonas viridis* consists of four protein subunits, called cytochrome, L, M, and H. In addition, it contains 14 major cofactors: four heme groups are covalently attached to the cytochrome subunit, two closely associated bacteriochlorophylls b (BCMP, BCLP), forming the so-called special pair (SP), two accessory chlorophylls b (BCMA, BCLA), two bacteriopheophytins (BPM, BPL), one menaquinone (Q_A), one ubiquinone (Q_B), a carotenoid (NS1), and a non-heme iron ion (FE1). Some of these cofactors are shown in Figure 1. Absorption of light by the special pair leads to its first excited singlet state. This excitation initiates a sequence of electron-transfer reactions from the special pair to the bacteriopheophytin BPL, to the primary quinone Q_A, and finally to the secondary quinone Q_B. The secondary quinone actually receives two electrons through this pathway, and from the cytoplasmic side of the protein it receives two protons. Q_BH_2 so formed leaves the reaction center.

The electron-transfer processes from the excited special pair to BPL, i.e., $SP^*BPL \rightarrow SP^+BPL^-$, and from BPL to the primary quinone Q_A, i.e., $BPL^-Q_A \rightarrow BPL\ Q_A^-$, occur on a time scale shorter than a nanosecond, i.e., on a time scale that is accessible to computer simulations.[7,8,10] Dynamics simulations of these processes have already been performed, leading to information about the structural response of the protein matrix to these electron-transfer steps, about the stabilization of the product state,[11,12] about the temperature dependence of transfer reactions,[13] and about the rate of quantum tunneling processes.[14,15]

In this contribution we focus on the electron-transfer step $Q_A^-Q_B \rightarrow Q_AQ_B^-$. Many experiments regarding this transfer step have been carried out, and the function of the Q_B binding site has been

* To whom correspondence should be sent.

(1) Leonhard, H.; Weller, A. *Z. Phys. Chem., Neue Folge* **1961**, *29*, 277; *Ber. Bunsen-Ges. Phys. Chem.* **1963**, *67*, 791.
(2) Deisenhofer, J.; Epp, O.; Miki, K.; Huber, R.; Michel, H. *Nature* **1985**, *318*, 618.
(3) Allen, J. P.; Feher, G.; Yeates, T. O.; Rees, D. C.; Deisenhofer, J.; Michel, H.; Huber, R. *Proc. Natl. Acad. Sci. U.S.A.* **1986**, *83*, 8589.
(4) McCammon, J. A. *Rep. Prog. Phys.* **1984**, *47*, 1.
(5) McCammon, J. A.; Harvey, S. C. *Dynamics of Proteins and Nucleic Acids*; Cambridge University Press: Cambridge, 1987.
(6) Brooks, C. L.; Karplus, M.; Pettitt, B. M. In *Advances in Chemical Physics*; Prigogine, I., Rice, S. A., Eds.; Wiley-Interscience: New York, 1988; Vol. 71.
(7) Kirmaier, C.; Holten, D. *Photosynth. Res.* **1987**, *13*, 225.
(8) Parson, W. W. In *New comprehensive biochemistry: Photosynthesis*; Amesz, J., Ed.; Elsevier: Amsterdam, 1987; pp 43.
(9) Boxer, S. G.; Goldstein, R. A.; Lockhart, D. J.; Middendorf, T. R.; Takiff, L. *J. Phys. Chem.* **1989**, *93*, 8280.
(10) Breton, J.; Martin, J. L.; Migus, A.; Antonetti, A.; Orszag, A. *Proc. Natl. Acad. Sci. U.S.A.* **1986**, *83*, 5121.
(11) Treutlein, H. Ph.D. Thesis, Technische Universität München, Munich, 1988.
(12) Treutlein, H.; Schulten, K.; Deisenhofer, J.; Michel, H.; Brünger, A.; Karplus, M. In *The photosynthetic bacterial reaction center: Structure and dynamics*; Breton, J., Vermeglio, A., Eds.; Plenum Press: London, 1988; pp 139.
(13) Tesch, M. Master's Thesis, Technische Universität München, Munich, 1989.
(14) Creighton, S.; Hwang, J.-K.; Warshel, A.; Parson, W. W.; Norris, J. *Biochemistry* **1988**, *27*, 775.
(15) Warshel, A.; Chu, Z. T.; Parson, W. W. *Science* **1989**, *246*, 112.

0022-3654/91/2095-2059$02.50/0

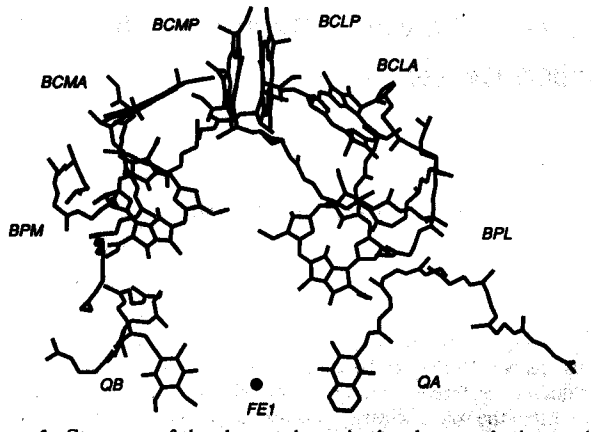

Figure 1. Structure of the chromophores in the photosynthetic reaction center of *Rhodopseudomonas viridis* with their abbreviated names.

investigated. A reaction scheme for the electron transfer and the quinone binding at the Q_B site of *Rhodopseudomonas sphaeroides* has been developed,[16,17] and the observed secondary site specificity for quinone binding has been shown to be governed by the free energy difference for the electron transfer.[18] ΔH and ΔG values for electron transfer in *Rhodopseudomonas sphaeroides* have been measured and are found to be strongly dependent on the nature of the quinones bound at the Q_A and Q_B sites.[19,20]

For *Rhodopseudomonas sphaeroides* the following pathway of quinone reduction has been proposed: after a first light pulse one electron is transferred to Q_B, forming a stable complex $Q_AQ_B^-$.[21] After a second light flash first a complex $Q_A^-Q_B^-$ is formed. Before the second transfer to Q_B^- occurs, this species is probably neutralized by protonation according to $Q_B^- + H^+ \rightarrow Q_BH$. This mechanism is consistent with the known mechanism of quinone reduction in aqueous solution[22] and avoids the problem that reduction of Q_B^-, i.e., $Q_B^- \rightarrow Q_B^{2-}$, generally requires too much energy and is unfavorable.[23]

The space between Q_A and Q_B in the photosynthetic reaction center is bridged by a non-heme iron (FE1 in Figure 1), which is ligated by histidines of the L (L190, L230) and M (M217, M264) subunits and by one glutamic acid (M232).[2] The function of the non-heme iron can be manyfold. As a 3d transition element iron has a strong affinity to undergo complexation. Its ligation by histidines L190 and M217 leads to a bridge between Q_A and Q_B, which might enhance the tunneling efficiency of an electron between Q_A and Q_B. The small fluctuations of the iron ion, as observed in the simulations, are indicative of a relatively strong ligation. The ion, in the case that it carries a net formal charge 2+ (the charge assumed in our simulation), would be involved in strong electrostatic interactions with Q_A and Q_B and the groups nearby. ESR studies have shown that both Q_A and Q_B interact with the iron atom,[24,25] generating a highly distorted and broadened EPR signal. The species $Q_A^-FeQ_B^-$, which can be formed at low temperature, exhibits no detectable EPR signal, indicating a coupling of the two spins.[26] After extraction of the iron, the transfer $Q_A^-Q_B \rightarrow Q_AQ_B^-$ in *Rhodopseudomonas sphaeroides* is slower by a factor of 2.3[27] and after removing the H-subunit the transfer is inhibited.[28]

An appropriate method to test the Q_B binding site is experiments with herbicides that replace the quinone bound to the Q_B site.[29] Crystal structures of reaction centers with bound herbicides are known, and herbicide binding sites have been analyzed.[29]

The transfer $Q_A^-Q_B \rightarrow Q_AQ_B^-$ is much slower than the primary transfers $SP^*BPL \rightarrow SP^+BPL^-$ and $BPL^-Q_A \rightarrow BPLQ_A^-$ and occurs on the time scale of microseconds to milliseconds.[16] Therefore, molecular dynamics simulations of fluctuations and relaxation accompanying the $Q_A^-Q_B \rightarrow Q_AQ_B^-$ transfer are beyond today's computing capacities.

We will adopt, therefore, the following procedures. In a first simulation (A), lasting 25 ps, we describe the state $Q_A^-Q_B$, i.e., the state before the transfer. In a second simulation (B), lasting 2 ps, the atomic partial charges of Q_A and Q_B are initially altered in accordance with a state $Q_AQ_B^-$. The second simulation describes then the response of the protein environment to the transfer $Q_A^-Q_B \rightarrow Q_AQ_B^-$ and the dielectric relaxation after the transfer. In a third simulation (C), lasting 20 ps, the equilibrium reached after the transfer is analyzed, e.g., average structure and atomic mobilities are determined. The coupling of the protein environment to the electron-transfer process is monitored through the energy $\Delta E(t)$ defined as the energy required for a *virtual* electron transfer, i.e., $Q_A^-Q_B \rightarrow Q_AQ_B^-$ in case of trajectory A and $Q_AQ_B^- \rightarrow Q_A^-Q_B$ in case of trajectory B.

We have also investigated in how far the non-heme iron is coupled to the $Q_A^-Q_B \rightarrow Q_AQ_B^-$ transfer. For this purpose we have carried out the same simulation as in cases A and B, except that an iron with a small mass of 1 au had been assumed. We will refer to these simulations as A′ and B′.

2. Method of Calculation

Our simulations are based on the X-ray structure of the photosynthetic reaction center of *Rhodopseudomonas viridis* at 2.3-Å resolution.[37] Charge distributions for the special pair, the accessory chlorophylls, and the bacteriopheophytins were taken from INDO calculations.[38] The partial charges of the two quinones Q_A and Q_B and the semiquinones Q_A^-, Q_B^- and Q_B^{2-} were calculated with the program package AMPAC[39] using the AM1 Hamiltonian.[40] The charge states for the amino acids are those for pH = 7, assuming standard pK values, except for glutamate L104 which was protonated. Molecular dynamics simulations have been carried out with the program XPLOR[41] using the CHARMM force field.[42]

To reduce the molecular dynamics simulations to a size that can be handled computationally, the stochastic boundary method[43,44] as implemented in XPLOR has been applied. This method

(16) Wraight, C. A. *Biochem. Biophys. Acta* **1979**, *548*, 309.
(17) Wraight, C. A.; Stein, R. R. In *The Oxygen Evolving System of Photosynthesis*; Inoue, Y., Crofts, A. R., Govindjee, Murata, N., Renger, G., Satoh, K., Eds.; Academic: New York, 1983; p 383.
(18) Giangiacomo, K. M.; Dutton, P. L. *Proc. Natl. Acad. Sci. U.S.A.* **1989**, *86*, 2658.
(19) Mancino, L. J.; Dean, D. P.; Blankenship, R. E. *Biochem. Biophys. Acta* **1984**, *764*, 46.
(20) Kleinfeld, D.; Okamura, M. Y.; Feher, G. *Biochem. Biophys. Acta* **1984**, *766*, 126.
(21) Pulles, M. P. J.; van Gorkom, H. J.; Willemsen, J. G. *Biochem. Biophys. Acta* **1976**, *449*, 536.
(22) Chambers, J. Q. In *The Chemistry of the Quinoid Compounds*; Parai, S., Ed.; Wiley-Interscience: New York, 1974; Vol. 2.
(23) Prince, R. C.; Dutton, P. L.; Bruce, J. M. *FEBS Lett.* **1983**, *160*, 273.
(24) Wraight, C. A. *Biochem. Biophys. Acta* **1977**, *459*, 525.
(25) Rutherford, A. W.; Heathcote, P.; Evans, M. C. W. *Biophys. J.* **1979**, *182*, 515.
(26) Wraight, C. A. *FEBS Lett.* **1978**, *93*, 283.
(27) Debus, R. J.; Feher, G.; Okamura, M. Y. *Biochemistry* **1986**, *25*, 2276.
(28) Okamura, M. Y.; Feher, G.; Nelson, N. In *Photosynthesis: Energy Conversion by Plants and Bacteria*; Govindjee, Ed.; Academic: New York, 1982; p 195.
(29) Michel, H.; Epp, O.; Deisenhofer, J. *EMBO J.* **1986**, *5*, 2445.
(30) Markham, J. J. *Rev. Mod. Phys.* **1959**, *31*, 956.
(31) Tesch, M.; Schulten, K., submitted to *J. Chem. Phys.*
(32) Marcus, R. A.; Sutin, N. *Biochem. Biophys. Acta* **1985**, *811*, 265.
(33) Hopfield, J. *Proc. Natl. Acad. Sci. U.S.A.* **1974**, *71*, 3640.
(34) DeVault, D. *Quantum-Mechanical Tunneling in Biological Systems*, 2nd ed.; Cambridge University Press: Cambridge, 1984.
(35) Bittl, R.; Schulten, K. *J. Chem. Phys.* **1989**, *90*, 1794.
(36) Kirmaier, C.; Gaul, D.; DeBey, R.; Holten, D.; Schenk, C., submitted to *Science*.
(37) Deisenhofer, J.; Epp, O.; Sinning, I.; Michel, H., manuscript in preparation.
(38) Plato, M.; Lendzian, F.; Lubitz, W.; Tränkle, E.; Möbius, K. In *The Photosynthetic Bacterial Reaction Center: Structure and Dynamics*; Breton, J., Vermeglio, A., Eds.; Plenum Press: London, 1988; p 379.
(39) Dewar, M. J. S.; Stewart, J. J. P. *QCPE Bull.* **1986**, *6*, 24.
(40) Dewar, M. J. S.; Zoebisch, E. G.; Healy, E. F.; Stewart, J. J. P. *J. Am. Chem. Soc.* **1985**, *107*, 3902.
(41) Brünger, A. T. In *Crystallographic computing 4: Techniques and new technologies*; Isaacs, N. W., Taylor, M. R., Eds.; Clarendon Press: Oxford, 1988.
(42) Brooks, B. R.; Bruccoleri, R. E.; Olafson, B. D.; States, D. J.; Swaminathan, S.; Karplus, M. *J. Comput. Chem.* **1983**, *4*, 187.
(43) Berkowitz, M.; McCammon, J. A. *Chem. Phys. Lett.* **1982**, *90*, 215.

divides the simulated protein into three regions. A first inner region, a sphere centered at the non-heme iron and containing all the atoms within a radius of 26.5 Å, is described by conventional molecular dynamics. The chromophores involved in electron transfer (SP, BCLA, BPL, Q_A, and Q_B as well as BCMA and BPM) are contained in this region, together with 4207 atoms. In a second region, within a spherical shell around the first region with inner and outer radii of 26.5 and 29.0 Å, respectively, atomic motion is treated by Langevin dynamics, introducing thermal and frictional effects of a surrounding bath. This region contained 644 atoms. A third region, a spherical shell around the first two regions with inner and outer radii of 29.0 and 37.5 Å, respectively, was not simulated explicitly. Coulomb interactions of charged amino acids located in this region with atoms in the two inner regions were taken into account by representing each charged amino acid through a single, fixed point charge.

The first and second region together contained 5315 atoms, including 83 water molecules detected in the X-ray structure. Simulations have been carried out with an integration step size of 1 fs applying the SHAKE algorithm.[45] Simulations with a "light" iron ion with a mass of 1 au were carried out with an integration step size of only 0.5 fs without application of SHAKE.

Dielectric fluctuations and relaxation accompanying electron transfer were monitored by calculating the expression $\Delta E(t) = E_P(t) - E_R(t)$, where $E_R(t)$ and $E_P(t)$ denote the Coulomb energies of the reaction center with chromophore charge distributions according to the reactant and product state, respectively. Before the electron transfer, $\Delta E(t)$ corresponds to the energy required to transfer an electron from the reactant to the product state when the protein motion corresponds to that for a charge distribution of the reactant state. After the electron transfer, $-\Delta E(t)$ is the energy required for transfer of an electron from the product state to the reactant state when the protein motion corresponds to that for a charge distribution of the product state. We denote the mean value of $\Delta E(t)$ before the transfer as $\langle \Delta E \rangle_{Q_A^- Q_B}$ and the corresponding value after the transfer as $\langle \Delta E \rangle_{Q_A Q_B^-}$. Data sampling took place in the following way: after equilibration, a 25-ps simulation (trajectory A) was run applying the charge distribution for the reactant state. In intervals of 10 fs the energy $\Delta E(t)$ for a virtual transfer was determined as follows: for the momentaneous protein configuration the total Coulomb energy in the $Q_A^- Q_B$ state, $E_R(t)$, as well as in the state $Q_A Q_B^-$, $E_P(t)$, were determined, and $\Delta E(t) = E_P(t) - E_R(t)$ was evaluated. Thus $\Delta E(t)$ corresponds to the energy required for *instantaneous* electron transfer. The procedure described was adopted also for trajectories B and C.

3. Formal Description of the Coupling between Protein Motion and Electron Transfer

In this section we will outline how thermal fluctuations in $\Delta E(t)$ control electron transfer. We will adapt for this purpose existing theories of electron transfer in solution.[32-34] The starting point of our consideration is the fact that our molecular dynamics calculations treat the protein classically. Such a description suffices for low-frequency motions, but not for intramolecular high-frequency motions. Furthermore, the simulations do not account for intramolecular and Born energy type contributions to the redox energy. Hence, we can expect to describe by our simulations only a contribution to the electron-transfer rate that is due to coupling of the transfer process to the protein environment. To account for this limitation, we represent the electron-transfer rate formally through the following convolution integral:

$$k_{tot} = \int_{-\infty}^{\infty} d\epsilon \; k_{cl}(\epsilon) \cdot S_{qm}(-\epsilon) \qquad (1)$$

This representation assumes that two classes of motions couple to the electron transfer, a class of quantum mechanical motions described by a line-shape function $S_{qm}(E)$ and a class of classical motions that give rise to the energy-transfer rate $k_{cl}(E)$. The two classes of motions exchange energy ϵ and $-\epsilon$ during the transition, the sum of energies exchanged being zero since electron transfer is a thermal process, i.e., does not require external energy, except thermal energies exchanged with a heat bath, an exchange that is included in calculating $S_{qm}(E)$ and $k_{cl}(E)$.

In keeping with the character of molecular dynamics simulations we will focus on the properties of the classical contribution and assume that the quantum mechanical degrees of freedom give rise to an unspecified line-shape function $S_{qm}(E)$. However, for the sake of completeness we outline the properties of $S_{qm}(E)$ for the case that the quantum degrees of freedom are harmonic. The line-shape function $S_{qm}(E)$ is then the Franck–Condon and Boltzmann-weighted energy density of final states given by the convolution

$$S_{qm}(E) = \int dE_1 \int dE_2 \cdots \int dE_N [\prod_{j=1}^{N} S_j(E_j)] \delta(\sum_{j=1}^{N} E_j - E - E_{redox\text{-}Born}) \qquad (2)$$

Each of the line-shape functions $S_j(E)$ describes a single degree of freedom and is[30]

$$S_j(E) = \frac{e^{-s_j(1+2n_j)}}{\hbar\omega_j} \left(\frac{n_j + 1}{n_j} \right)^{(E-E_{0j})/2\hbar\omega_j} \sum_{k=-\infty}^{\infty} \delta\left(k - \frac{E - E_{0j}}{\hbar\omega_j} \right) I_{(E-E_{0j})/\hbar\omega_j}(2s_j\sqrt{n_j(n_j+1)}) \qquad (3)$$

where $s_j = {}^1/_2 f_j q_j^2/\hbar\omega_j$ is the so-called reorganization energy in units of vibrational quanta and $n_j = e^{-\hbar\omega_j/kT}/(1 - e^{-\hbar\omega_j/kT})$ is the average number of quanta thermally excited in the oscillator. The quantum mechanical line-shape function also accounts for the electronic and Born contributions to the redox energy $E_{redox\text{-}Born}$.

We have presented the roles of quantum and classical degrees of freedom in (1) in an asymmetric way. In fact, in (1) the coupling of the classical degrees of freedom to electron transfer, in principle, is described exactly, whereas the quantum degrees of freedom enter through the final state density $S_{qm}(E)$ in a manner similar to their appearance in Fermi's golden rule. A description that applies the latter approximation to both classical and quantum mechanical degrees of freedom yields the transfer rate

$$k_{tot} = \frac{2\pi|V_{el}|^2}{\hbar} \int_{-\infty}^{\infty} d\epsilon \; S_{cl}(\epsilon) \cdot S_{qm}(-\epsilon) \qquad (4)$$

where $S_{cl}(\epsilon)$ is a classical line-shape function and where V_{el} describes the electronic coupling matrix element between reactant and product states, i.e., in the present case between $Q_A^- Q_B$ and $Q_A Q_B^-$.

In order to describe, as required to apply (1), the coupling between the classical nuclear degrees of freedom and electron transfer exactly, a description is needed that expresses the corresponding coupling. Such coupling is provided by a model that describes the electronic quantum system by a two-state Hamiltonian:

$$H_{el}(\epsilon) = \begin{pmatrix} \epsilon & V_{el} \\ V_{el} & \Delta E(t) \end{pmatrix} \qquad (5)$$

where ϵ is the energy "exchanged" with the quantum mechanical nuclear and electronic degrees of freedom and where the energy difference $\Delta E(t)$ describes the coupling and thermal motion of the classical degrees of freedom. The electron transfer can then be described by a 2×2 density matrix ρ that obeys the Liouville equation

$$\partial_t \rho(\epsilon|t) = \frac{i}{\hbar}[H_{el}(\epsilon)\, \rho(\epsilon|t)]_- - [K, \rho(\epsilon|t)]_+,$$

$$K = \begin{pmatrix} 0 & 0 \\ 0 & \tau^{-1} \end{pmatrix}, \quad \rho(\epsilon|0) = \begin{pmatrix} 1 & 0 \\ 0 & 0 \end{pmatrix} \qquad (6)$$

Here we employed the notation $[A,B]_\pm = AB \pm BA$. τ^{-1} measures the relaxation of the system in the product state $Q_A Q_B^-$, i.e.,

(44) Brünger, A. T.; Huber, R.; Karplus, M. *Biochemistry* **1987**, *26*, 5153.
(45) van Gunsteren, W. F.; Berendsen, H. J. C. *Mol. Phys.* **1977**, *34*, 1311.

essentially the rate of solvation of the state after electron transfer. $\rho_{11}(\epsilon|t)$ gives the probability of finding the system at time t in the (initial) reactant state $Q_A^-Q_B$. Assuming for the sake of approximation a monoexponential decay of the initial state, the electron-transfer rate is approximately

$$k_{el}^{-1}(\epsilon) = \int_0^\infty dt\, \rho_{11}(\epsilon|t) \tag{7}$$

This transfer time has been determined in ref 31 for the primary and secondary electron transfers in the photosynthetic reaction center by solving eq 6.

$\Delta E(t)$ introduced above is evaluated as the energy difference between the charge state, e.g., $Q_A^-Q_B$, for which a classical trajectory of the protein is evaluated, and a virtual charge state, e.g., $Q_AQ_B^-$. It is obvious that the properties of $\Delta E(t)$ influence the electron-transfer rate, an influence that would be described quantitatively by solving the evolution equation for the density matrix of the two-state system.

We now discuss which features of $\Delta E(t)$ are relevant in determining the transfer rate. For this purpose we assume momentarily for the purpose of argument that the classical degrees of freedom are also harmonic and that their influence can be accounted for by a line-shape function as in (4). In this case the line-shape function is given by the convolution

$$S_{el}(\Delta E) = \int dE_1 \int dE_2 \cdots \int dE_{N'} [\prod_{j=1}^{N'} S_j(E_j)]\delta(\sum_{j=1}^{N'} E_j - \Delta E) \tag{8}$$

The single mode contributions are[32]

$$S_j(E) \sim \frac{1}{\sqrt{2\pi\sigma_j f_j^2 q_{0j}^2}} \exp\left(-\frac{(E_{0j} + \frac{1}{2}f_j q_{0j}^2 - E)^2}{2f_j^2 q_{0j}^2 \sigma_j}\right) \tag{9}$$

where

$$\sigma_j = kT/f_j \tag{10}$$

The line-shape function (8) can be identified with the normalized distribution of $\Delta E(t)$ values resulting from a molecular dynamics simulation. This distribution can be expressed by the single Gaussian

$$S_{el}(\Delta E) = (1/\sqrt{\pi\Sigma}) \exp(-(\langle \Delta E\rangle - \Delta E)^2/\Sigma) \tag{11}$$

where

$$\Sigma = \sum_{j=1}^{N'} 1/2 f_j^2 q_{0j}^2 \sigma_j, \quad \langle \Delta E\rangle = \sum_{j=1}^{N'} (E_{oj} + \tfrac{1}{2}f_j q_{0j}^2) \tag{12}$$

According to the central limit theorem[46] one can argue that even in the case where the individual classical degrees of freedom are not harmonic and, therefore, not accounted for by Gaussian-type line-shape functions (9), the convolution of many line-shape functions, irrespective of their exact form, should still yield a Gaussian like (11). For this property to hold, the line-shape functions $S_j(E)$ contributing in (8) must obey the Lindeberg condition,[46] a weak condition that requires that the wings of $S_j(E)$ decay rapidly enough. In fact, our simulations discussed below yield a distribution $S_{el}(\Delta E)$ that can be well represented by a Gaussian line shape.

The simulations presented below reveal that an electron transfer is accompanied by a change of the mean value $\langle \Delta E\rangle$ from a value $\langle \Delta E\rangle_{Q_A^-Q_B}$ before the transfer to a value $\langle \Delta E\rangle_{Q_AQ_B^-}$ after the transfer. One can show that the overall effect of the classical degrees of freedom on $\Delta E(t)$ can be accounted for by effective energy potentials for reactant and product states that are consistent with a Gaussian line-shape function. The corresponding potential functions are exactly those assumed in the Marcus theory of electron transfer, namely, two displaced harmonic potentials with identical force constants:

$$E_R(q) = \tfrac{1}{2}fq^2, \quad E_P(q) = \tfrac{1}{2}f(q - \Delta)^2 + \Delta E_0 \tag{13}$$

(46) Gardiner, C. W. *Handbook of Stochastic Methods*, Springer: New York, 1983; pp 37.

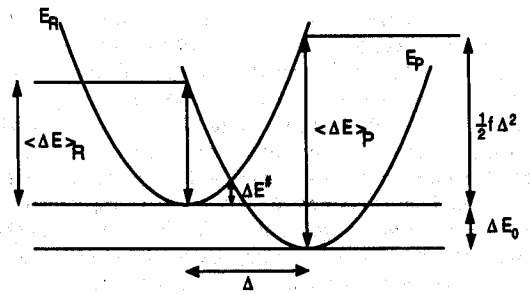

Figure 2. Representation of the multidimensional potential surfaces of reactants E_R and products E_P according to the Marcus theory as a function of a nontrivial reaction coordinate. Δ is the displacement of the two parabolas that represent the potential surfaces, k represents a force constant, λ is the reorganization energy, and $\Delta E^\#$ is the activation energy for the electron transfer.

depicted in Figure 2. Here q represents a coordinate that describes the effective coupling of the nuclear degrees of freedom to $\Delta E(t)$, i.e., to virtual electron transfer. The potentials are determined by the three parameters f, Δ, and ΔE_0. To derive the relationship between these parameters and Σ, $\langle \Delta E\rangle_{Q_A^-Q_B}$ and $\langle \Delta E\rangle_{Q_AQ_B^-}$ we start from the Boltzmann distribution $p_B(q) = \sqrt{f/2\pi kT}\exp(-fq^2/2kT)$ in the reactant potential and note that the energy difference between product and reactant states is $\Delta E(q) = E_P(q) - E_R(q) = fq\Delta + \Delta E_0 + {}^1/_2f\Delta^2$, the inversion of which yields $q(\Delta E) = (\Delta E - \Delta E_0 - {}^1/_2f\Delta^2)/f\Delta$. Inserting this into the expression of the classical line-shape function $S_{el}(\Delta E) = p_B(q(\Delta E))|dq/d\Delta E|$ yields with the Jacobian $|dq/d\Delta E| = f\Delta$ the result $S_{el}(\Delta E) = (2\pi fkT\Delta^2)^{-1/2}\exp(-(\Delta E - \Delta E_0 - {}^1/_2f\Delta^2)^2/2fkT\Delta^2)$. One can then identify by comparing this expression with (11) and (12)

$$\Sigma = 2fkT\Delta^2 \tag{14}$$

$$\langle \Delta E\rangle_{Q_A^-Q_B} = {}^1/_2f\Delta^2 + \Delta E_0 \tag{15}$$

$$\langle \Delta E\rangle_{Q_AQ_B^-} = -{}^1/_2f\Delta^2 + \Delta E_0 \tag{16}$$

The three conditions (14)–(16) allow one to determine the potential surfaces (13) shown in Figure 2 from the quantities Σ, $\langle \Delta E\rangle_{Q_A^-Q_B}$, and $\langle \Delta E(t)\rangle_{Q_AQ_B^-}$ available through molecular dynamics simulations (see section 4.2). Actually, simulations yield slightly different values for the variance of the fluctuations of $\Delta E(t)$ before (Σ_R) and after (Σ_R) electron transfer. However, in the photosynthetic reaction center the variances do not depend strongly on the charge state of the chromophores, and hence a single value suffices to characterize the effective potential surfaces of the system. This feature is very fortunate since it implies that $\Delta E(q) = E_P(q) - E_R(q)$ is a monotonous (and linear) function of q, a feature exploited by the Marcus theory.

At this point it should be noted that the quantities Σ, $\langle \Delta E\rangle_{Q_A^-Q_B}$, $\langle \Delta E\rangle_{Q_AQ_B^-}$, and therefore also f, Δ, and ΔE_0, i.e., the potentials in Figure 2, can be found to vary with temperature. In fact, a significant temperature variation of these quantities has been observed in case of a simulation of the two transfers $SP\,BPL\,Q_A \rightarrow SP^+\,BPL^-\,Q_A \rightarrow SP^+\,BPL\,Q_A^-$.[31]

Actually, the coordinate q used in depicting the potential curves $E_R(q)$ and $E_P(q)$ is only implicitly needed for a description of electron transfer. All that is explicitly needed for a quantum mechanical description of such transfer through the Hamiltonian (5) is knowledge of $\Delta E(t) = E_R(q(t)) - E_P(q(t))$, which results from the thermal motion of the protein, the explicit q coordinate being irrelevant. If one assumes that the thermal motion is Brownian, one can seek a stochastic model that reproduces the line-shape function (11). Such a model is provided through the Fokker–Planck equation

$$\partial_t p(\Delta E,t) = D\,\partial_{\Delta E} S_{el}(\Delta E)\,\partial_{\Delta E}[S_{el}(\Delta E)]^{-1}\,p(\Delta E,t) \tag{17}$$

which describes the probability to observe an energy ΔE (for virtual electron transfer) at time t. One can prove that the probability distribution $p(\Delta E,t)$ asymptotically converges toward the line-shape function, i.e.

$$\lim_{t\to\infty} p(\Delta E,t) = S_{cl}(\Delta E) \tag{18}$$

The Fokker–Planck equation (17) entails the constant D, which accounts for the random dynamics. For the Gaussian form of $S_{cl}(\Delta E)$ this quantity determines the energy–energy correlation function in a simple manner:

$$C_{\Delta E\Delta E}(t) = \frac{\langle(\Delta E(t_0+t) - \langle\Delta E\rangle)^2\rangle}{\langle(\Delta E(t_0) - \langle\Delta E\rangle)^2\rangle} = e^{-2Dt/\Sigma^2} \tag{19}$$

This correlation function can also be determined through a molecular dynamics simulation. One can then establish the stochastic model (17) by monitoring $\Delta E(t)$ in a molecular dynamics simulation, determine numerically the corresponding distribution function (11) and correlation function (19), and match the quantities Σ, ΔE_0, and D.

A stochastic model has considerable advantages over using in a quantum mechanical description $\Delta E(t)$ directly as obtained from a simulation. The first reason is that the simple formulation in terms of three parameters allows one to compare different electron transfer systems. The second reason is that the stochastic model considered allows one to represent the electron-transfer rate $k_{cl}(\epsilon)$ in a simple and transparent form. This representation has been derived in ref 35. Employing the expression (7) the theory in[35] yields

$$k^{-1}(\epsilon) = \int_0^\infty dt \left(\int dE' \exp\left[-\frac{it}{\hbar} \begin{pmatrix} \epsilon & V_{el} \\ V_{el} & E' - \frac{i\hbar}{\tau} \end{pmatrix} \right] \times \begin{pmatrix} 1 & 0 \\ 0 & 0 \end{pmatrix} \exp\left[\frac{it}{\hbar} \begin{pmatrix} \epsilon & V_{el} \\ V_{el} & E' + \frac{i\hbar}{\tau} \end{pmatrix} \right] \right)_{11} I(E') \tag{20}$$

where $I(E')$ represents the Kubo line-shape function

$$I(E') = \frac{1}{\pi} \mathrm{Re} \left\langle \frac{1}{D\,\partial_{\Delta E} S_{cl}(\Delta E)\,\partial_{\Delta E}[S_{cl}(\Delta E)]^{-1} + (i/\hbar)(\Delta E - E')} \right\rangle \tag{21}$$

This expression is actually an approximation, accurate to third order in V_{el}, the representation conserving the trace of the density matrix and converging to the exact results in the limits of both slow and fast stochastic motion.

One can write (20) as

$$k^{-1}(\epsilon) = \int dE'\, \hat{k}^{-1}(\epsilon - E')\, I(E') \tag{22}$$

where

$$\hat{k}^{-1}(\epsilon - E') = \int_0^\infty dt \left(\exp\left[-\frac{it}{\hbar} \begin{pmatrix} \epsilon & V_{el} \\ V_{el} & E' - \frac{i\hbar}{\tau} \end{pmatrix} \right] \begin{pmatrix} 1 & 0 \\ 0 & 0 \end{pmatrix} \times \exp\left[\frac{it}{\hbar} \begin{pmatrix} \epsilon & V_{el} \\ V_{el} & E' + \frac{i\hbar}{\tau} \end{pmatrix} \right] \right)_{11} \tag{23}$$

is the electron-transfer time for a time-independent Hamiltonian, i.e., one with $\Delta E(t) = E'$. The description provided by (22) and (24) can be readily interpreted. The rate $\hat{k}(\epsilon - E')$ is strongly peaked at $\epsilon = E'$ with a typical width of about 10^{-3} eV determined by either V_{el} or $\hbar/\tau$, whichever is larger. However, the width of the Kubo line-shape function $I(E')$ is determined by the spectrum of the Fokker–Planck operator in (17) and by Σ, which leads to a bell-shaped ϵ dependence of $k(\epsilon)$ with a width of a few tenths of an electronvolt. This behavior, which is close to that described by the Marcus theory of electron transfer, has been discussed in more detail in ref 31. This reference also provides quantum mechanical calculations of transfer rates in the photosynthetic reaction center together with a detailed discussion of the ϵ dependence. Also an expression for the transfer rate, which is numerically more suitable than eq 22, is introduced. Such ϵ dependence implies that the intramolecular redox energy is not required to be tuned exactly to an optimal value, but rather that changes of the redox energies of the chromophores engaged in the electron transfer can be accommodated. The recent finding by Kirmaier et al.[36] that the chromophore BPL (bacteriopheophytin) in the photosynthetic reaction center of *Rh. sphaeroides* can be exchanged for a bacteriochlorophyl with a change in redox energy of about 0.2 eV, however, with a minor concomitant change in the electron-transfer rate, attests to our conclusion.

In our analysis of molecular dynamics simulations below we will focus on the quantities that are relevant in the context of the electron-transfer theory outlined. We will discuss the behavior of $\Delta E(t)$ and of the corresponding distribution $S_{cl}(\Delta E)$ as well as consider the energy–energy correlation function.

4. Results and Discussion

1. Structure of the Reaction Center with Q_A^-. Starting from the X-ray structure the chosen segment of the reaction center has been equilibrated at 300 K for 15 ps. The charge distribution assumed represents a reaction center with a neutral special pair and a primary menaquinone with a charge of −1. A neutral special pair has been chosen because the time needed for neutralization of SP^+ is $\tau \simeq 0.2$ μs,[32] which is shorter than the time, $\tau \simeq 200$ μs, for the transfer $Q_A^-Q_B \rightarrow Q_AQ_B^-$ in *Rhodopseudomonas sphaeroides*.[47] Following the equilibration a 25-ps trajectory A has been calculated. The results of this simulation will be presented now.

We first investigated the average structure resulting for trajectory A. We found that the X-ray structure was largely preserved; the mean deviation between our average structure and the X-ray structure, represented in the form of a root-mean-square (rms) value, is 2.0 Å for all the atoms and 1.1 Å for all the C^α atoms. These values are, however, larger than those found in previous simulations for neutral chromophores[11] with corresponding rms values of 1.06 and 0.63 Å, respectively. The structural differences are believed to be mainly an effect of the different charge distribution since the X-ray structure corresponds to chromophores in the neutral state. Differences to the calculation reported in ref 11 could also appear due to the selection of another segment of the reaction center in the present simulation.

An interesting feature of the average structure of run A is a shortening of the distance between Q_A and FE1 by about 0.4 Å relative to the distance found in the X-ray structure. The closer distance should be due to the electrostatic interaction between the positively charged FE1 (+2) and Q_A^-. Since the electron transfer between $Q_A^-Q_B$ and $Q_AQ_B^-$ involves electron tunneling and, therefore, would be strongly affected by the edge-to-edge distance between Q_A and Q_B, a closer FE1–Q_A distance and, simultaneously, a closer Q_A–Q_B distance may prepare the reaction center for the following electron transfer $Q_A^-Q_B \rightarrow Q_AQ_B^-$.

In this context it may be interesting to examine the fluctuations of the distance between Q_A^- and Q_B. The center-to-center distance observed during a trajectory of 25 ps is shown in Figure 3. The distance shows smaller fluctuations with sporadic large deviations from the mean distance of more than ±0.6 Å. On a longer time scale even larger displacements may occur. Therefore, these fluctuations could strongly influence the electronic matrix element between Q_A^- and Q_B. Consequently, the rate-limiting step for the electron transfer $Q_A^-Q_B \rightarrow Q_AQ_B^-$ could be an appropriate fluctuation of the edge-to-edge distance or other structural rearrangements of the groups, e.g., of the non-heme iron and of the histidines L190 and M217, bridging the gap between Q_A and Q_B.

We have determined also the atomic mobilities of trajectory A. These mobilities are presented in Figure 4. The values are quite different from those previously determined for reaction centers with neutral chromophores and for reaction centers with

(47) Crofts, A. R.; Wraight, C. A. *Biochem. Biophys. Acta* **1983**, *726*, 149.

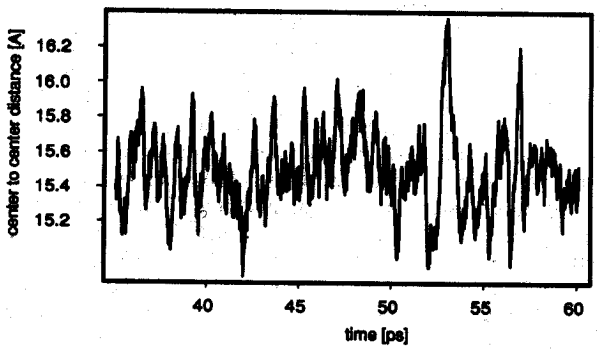

Figure 3. Fluctuation of the center-to-center distance between Q_A^- and Q_B during run A.

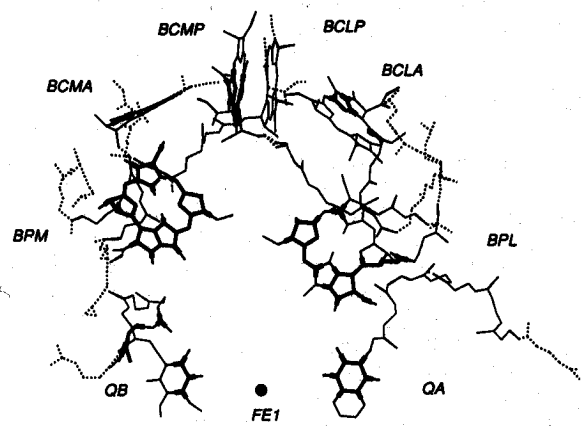

Figure 4. Mobilities of the chromophores calculated from a trajectory with a negative charged Q_A. Black, rms < 0.4; thin black, 0.4 < rms < 0.7; thin black dashed, rms > 0.7.

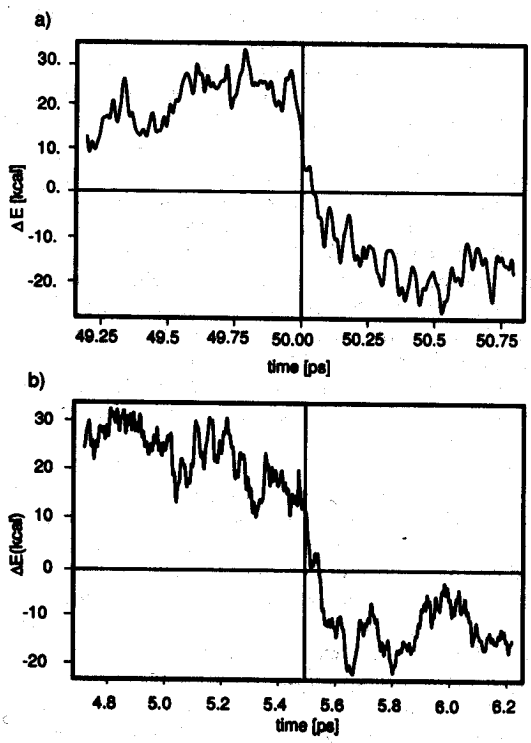

Figure 5. (a) $\Delta E(t)$ accompanying the electron transfer $Q_A^-Q_B \rightarrow Q_AQ_B^-$. (b) $\Delta E(t)$ calculated from a trajectory with a "light" iron ion, i.e., an iron atom with a mass of 1 au. The charge distribution has been altered at 50.00 ps (a) and at 5.5 ps (b) corresponding to a $Q_A^-Q_B \rightarrow Q_AQ_B^-$ transition.

chromophores in the $SP^+BPL^-Q_AQ_B$ state.[12] The special pair in the $SP\,BPLQ_A^-Q_B$ state is much more flexible than in simulations involving a neutral Q_A, i.e., $SP\,BPLQ_AQ_B$ and $SP^+BPL^-Q_AQ_B$ states, whereas the quinones are remarkably stiff. The latter

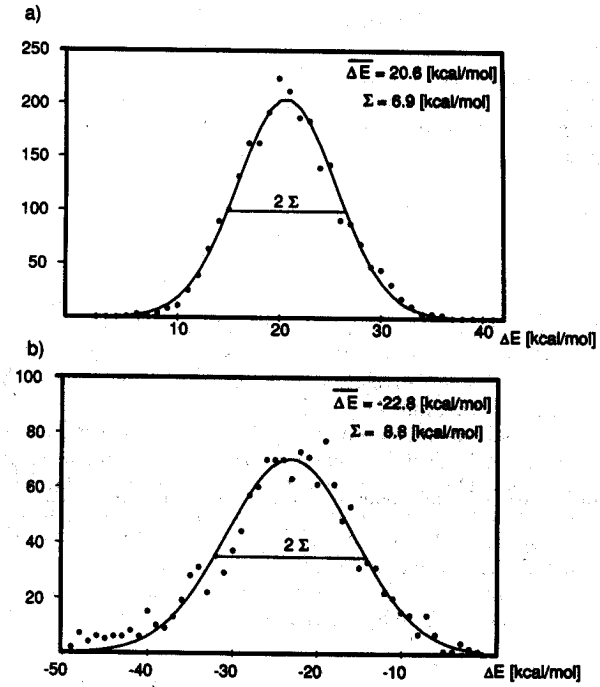

Figure 6. Distribution of $\Delta E(t)$ values analyzed from trajectory A (a) and from trajectory C (b).

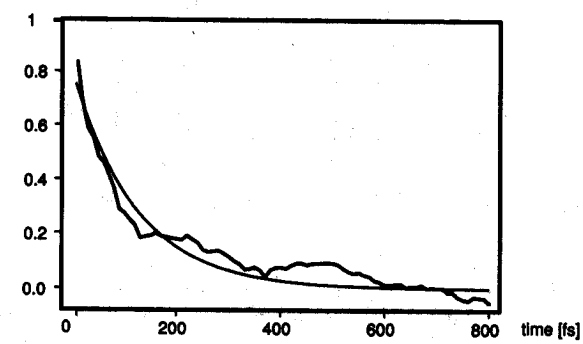

Figure 7. Time dependence of the energy–energy correlation function $C_{\Delta E\Delta E}(t)$ (19) determined from trajectory A. The function has been matched to $\exp(-t/\tau)$ for τ = 120 fs.

observation seems to contradict the assumption made above that structural fluctuations involving the Q_A^--Q_B edge-to-edge distance could be central to the transfer $Q_A^-Q_B \rightarrow Q_AQ_B^-$. These mobilities, however, represent dynamical properties only on a short time scale of 20 ps, and the few large deviations have only a minor influence of the overall rms value.

2. Simulation of Electron Transfer to Q_B. As explained in section 3 the electron transfer in a protein is controlled to an important degree by fluctuations of $\Delta E(t)$ due to classical motion of the nuclear degrees of freedom. In Figure 5a we present these fluctuations resulting from our simulations (see Method of Calculation) for the final 1 ps of trajectory A. The fluctuations of $\Delta E(t)$ were monitored during the entire 20-ps time period of trajectory A. The resulting distribution of ΔE values is shown in Figure 6a. This distribution can be matched well to a Gaussian distribution as expected from the central limit theorem (see section 3) and assumed by the Marcus theory. The corresponding parameters are $\Sigma_{Q_A^-Q_B}$ = 6.9 kcal/mol and $\langle \Delta E \rangle_{Q_A^-Q_B}$ = 2.06 kcal/mol. We have also analyzed for trajectory A the decay of the energy–energy correlation function $C_{\Delta E\Delta E}(t)$ defined in (19). The correlation function is presented in Figure 7. Shown is also a match to an exponential $\exp(-t/\tau)$ from which a decay time τ of 120 fs is obtained.

As outlined above, the quinones in the reaction center were recharged at the end of trajectory A corresponding to a $Q_A^-Q_B \rightarrow Q_AQ_B^-$ transfer, and trajectory B started. The $\Delta E(t)$ values resulting from this trajectory during a period of 1 ps, immediately

after the electron transfer, are also presented in Figure 5. One observes clearly that $\Delta E(t)$ before electron transfer (recharging of quinones) fluctuates around an average value of about 20 kcal/mol, exhibits a response to the transfer through a very rapid relaxation process completed within about 200 fs, and resumes then fluctuations around a new average value of about −23 kcal/mol.

We have analyzed the fluctuations of $\Delta E(t)$ after electron transfer during the 20-ps time period of trajectory C. The distribution of ΔE values are presented in Figure 6b. Like for the distribution in Figure 6a, a Gaussian can be matched well, the parameters being $\Sigma_{Q_AQ_B^-} = 8.8$ kcal/mol and $\langle \Delta E \rangle_{Q_AQ_B^-} = -22.8$ kcal/mol. It is of particular interest to notice that the values $\Sigma_{Q_A^-Q_B}$ and $\Sigma_{Q_AQ_B^-}$ differ only by 1.9 kcal/mol, i.e., by 20%, which is sufficiently close to allow the assumption of identical (same f values) harmonic potentials $E_R(q)$ and $E_P(q)$ in the Marcus type presentation of the line-shape function $S_{cl}(\Delta E)$ as outlined in section 3.

According to the fluctuation–dissipation theorem a relationship between equilibrium correlation functions and response functions exists.[48] Applied to the correlation function $C_{\Delta E \Delta E}(t)$ the theorem states[48]

$$C_{\Delta E \Delta E}(t) = R_{\Delta E \delta}(t), \quad t \geq 0 \tag{24}$$

$$E = [S_{cl}(\Delta E)]^{-1} \delta S_{cl}(\Delta E) \tag{25}$$

where the differential operator $\delta = \Sigma/2\, \partial/\partial \Delta E$ in the framework of the Fokker–Planck equation (17) accounts for a perturbation for which $R_{\Delta E \delta}(t)$ describes the response. Adding δ to the Fokker–Planck operator $D\, \partial_{\Delta E} S_{cl}(\Delta E)\, \partial_{\Delta E} [S_{cl}(\Delta E)]^{-1}$ reveals that δ corresponds to a time-independent displacement of the equilibrium value $\langle \Delta E \rangle$, i.e., to the same situation that arises through electron transfer as shown in Figure 5. Hence, one expects that the decay times of $C_{\Delta E \Delta E}(t)$ in Figure 7 are the same as the decay of $R_{\Delta E \delta}(t)$ corresponding to Figure 5. In fact, an inspection of Figures 5a and 7 shows that the relaxation phenomena depicted are governed by nearly identical relaxation times. The difference in relaxation times assigned are most likely due to the poor statistics of the simulation data and due to the fact that the equivalence stated by the fluctuation–dissipation holds only in the limit of linear response theory, i.e., for small perturbations; the perturbation due to a charge displacement between Q_A and Q_B might not be small.

The relaxation process after electron transfer corresponds to a solvation of the charged chromophores by the protein matrix.[49] Previous simulations[50] have shown that the contributions to this relaxation due to the long range of the Coulomb interactions cannot be assigned to specific groups but rather are distributed between backbone, side chains, and chromophores.

To elucidate a possible effect of the motion of the photosynthetic reaction center's non-heme iron on the electron transfer, simulations with a light "iron" of a mass of 1 au have been performed (trajectories A′ and B′). The corresponding behavior of $\Delta E(t)$, i.e., fluctuations and relaxation, of $\Delta E(t)$ over a 1.5-ps time period are also presented in Figure 5. One observes that the behavior is similar to that of trajectory A, B: average values before and after transfer and amplitudes of fluctuation are similar for trajectories A, B and A′, B′. In particular, the extreme isotopic replacement does not affect the fast response of the system after electron transfer. We can conclude, therefore, that the function of the iron ion is mainly of electrostatic (attraction of Q_A^- and of Q_B^-) and electronic nature (d orbitals involved in electron transfer).

We want to demonstrate now that the energy values $\langle \Delta E \rangle_{Q_A^-Q_B}$ and $\langle \Delta E \rangle_{Q_AQ_B^-}$ are consistent with available experimental data on the free enthalpy differences between states $Q_A^-Q_B$ and $Q_AQ_B^-$. However, a difficulty in making a direct comparison between our

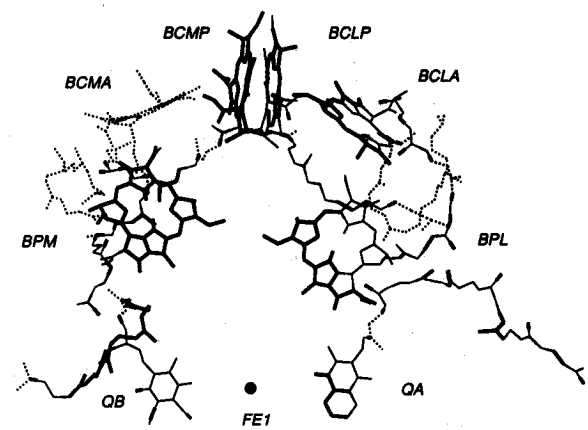

Figure 8. Structural changes due to the electron transfer $Q_A^-Q_B \rightarrow Q_AQ_B^-$. Black lines denote atom pairs with atoms the mean positions of which change by less than 0.4 Å. Atom pairs connected by thin black lines have their position shifted between 0.4 and 0.7 Å. Atoms connected by thin black dashed lines experience positional changes of more than 0.7 Å.

simulations and the observations arises because we presently describe only one of the contributing factors in (1), namely, $k_{cl}(\epsilon)$, and miss the other factor $S_{qm}(-\epsilon)$ which, in particular, accounts for the intramolecular redox energies and the Born energies. Since in the following we will consider only the differences in energy between states $Q_A^-Q_B$ and $Q_AQ_B^-$ and since the Born energy for both states should be nearly the same, the Born energy contributions are actually immaterial, but the redox energy difference is still required. This energy difference contributes to the term ΔE_0 of the potentials in Figure 2.

We start from relationships (15) and (16), from which we can infer

$$f\Delta^2 = \langle \Delta E \rangle_{Q_A^-Q_B} - \langle \Delta E \rangle_{Q_AQ_B^-} \tag{26}$$

$$\Delta E_0 = \langle \Delta E \rangle_{Q_A^-Q_B} + \langle \Delta E \rangle_{Q_AQ_B^-} \tag{27}$$

The corresponding value of 46.3 kcal/mol for $f\Delta^2$ is significantly larger than that determined from simulations of the transfer steps $SP^*BPL \rightarrow SP^+BPL^-$ or $BPL^-Q_A \rightarrow BPL\ Q_A^-$, the values found for the latter being 8.5[11] and 20.0 kcal/mol,[51] respectively. The value of ΔE_0 is −1.2 kcal/mol. Both values obtained for (26) and (27) should be rescaled by the inverse of the high-frequency contribution to the dielectric constant ϵ_∞ in the protein interior. Assuming $\epsilon_\infty = 2$, we obtain $f\Delta^2 = 23.2$ kcal/mol and $\Delta E_0 = -0.6$ kcal/mol. The latter value needs to be corrected for the redox energy difference of Q_A and Q_B, which according to ref 23 in DMF measures −2.8 kcal/mol. This results in an overall free enthalpy difference of −3.4 kcal/mol, which is in agreement with measured ΔH values for *Rhodopseudomonas sphaeroides* lying between −2.0 and −7.4 kcal/mol.[19,20,52]

The point of intersection $q^\#$ of $E_R(q)$ and $E_P(q)$ in Figure 2 within the approximate assumptions of the Marcus theory defines the activation energy for the process $Q_A^-Q_B \rightarrow Q_AQ_B^-$ according to $\Delta E^\# = E_R(q^\#)$. One obtains thereby the well-known expression

$$\Delta E^\# = \frac{\frac{1}{2} f\Delta^2 + \Delta E_0}{2f\Delta^2} \tag{28}$$

Using the rescaled and redox energy corrected values for these quantities, one obtains $\Delta E^\# = 1.9$ kcal/mol. This low value certainly is favorable for the transfer process; however, it might be at variance with the fact that the electron transfer $Q_A^-Q_B \rightarrow Q_AQ_B^-$ is quite slow. Since the time scale of our simulations is in the range of picoseconds and since proton uptake by the protein would occur on a longer time scale and is not considered in the calculation, comparison of our data with experimental results is difficult. A change in free energy connected with the transfer

(48) Risken, H. *The Fokker–Planck Equation*; Springer: New York, 1984.
(49) Maroncelli, M.; MacInnis, J.; Fleming, G. R. *Science* **1989**, *243*, 1674.
(50) Treutlein, H.; Schulten, K.; Deisenhofer, J.; Michel, H.; Brünger, A.; Karplus, M. *Proc. Natl. Acad. Sci. U.S.A.*, submitted for publication.
(51) Tesch, M.; Schulten, K. *Chem. Phys. Lett.* **1990**, *169*, 97.
(52) Wraight, C. A. Personal communication.

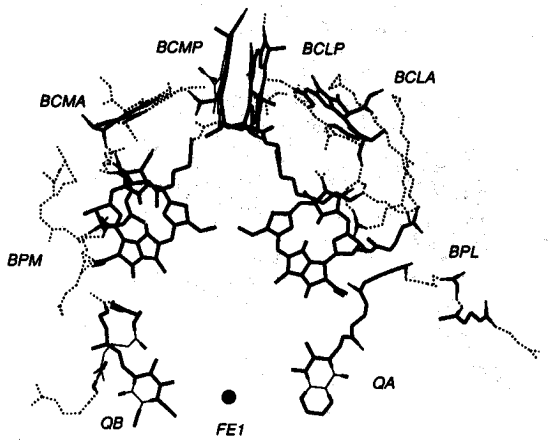

Figure 9. Mobilities of chromophore atoms after the electron transfer $Q_A^-Q_B \rightarrow Q_AQ_B^-$. Black, rms < 0.4; thin black, 0.4 < rms < 0.7; thin black dashed, rms < 0.7.

$Q_A^-Q_B \rightarrow Q_AQ_B^-$ could also be due to protonation of a group near the Q_B site, i.e., observed free enthalpy values may actually not relate solely to the energy difference resulting from our simulation.

3. Structure after the Electron Transfer to Q_B. After the electron transfer a 20-ps trajectory C with the new charge distribution was calculated and analyzed. Structural changes due to the new charge distribution are presented in Figure 8. These changes are generally quite small. Most of the chromophore atoms show displacements smaller than 0.4 Å due to the transfer $Q_A^-Q_B \rightarrow Q_AQ_B^-$. Coulomb interaction drives the ring system of Q_B^- by a short distance toward the positive iron ion Fe1. The mean distance between the center of Q_B^- and the iron changes from 9.05 to 8.55 Å, whereas the distance between the center of Q_A and the iron becomes longer by about 0.22 Å. We also monitored for trajectory C large displacements of the phytol chain atoms. These displacements are due to the generally high mobilities of these groups.

Atomic mobilities calculated from trajectory C are presented in Figure 9. These mobilities differ significantly from the ones calculated from trajectory A describing the $Q_A^-Q_B$ state. The special pair atoms are very stiff. The mobility of the special pair is similar to the one calculated with a positive charged special pair in the simulation of the transfer $SP^*BPL \rightarrow SP^+BPL^-$.[12] Since the "stiffness" of the chromophores seems to be an important requirement for an efficient electron transfer, the fact that the special pair becomes less mobile in the SP BPL Q_A Q_B^- state might be interpreted as a protein response that prepares the reaction center for a second transfer from the special pair to BPL.

4. Interactions at the Q_B Site. To derive some more insight into the mechanism of Q_B binding, we will have a closer look at the interactions of Q_B in various electronic states with its nearest neighbors. The electrostatic and van der Waals interaction energies with all residues within a sphere of radius 10 Å have been calculated for Q_B in the states $Q_A^-Q_B$, $Q_AQ_B^-$, $Q_A^-Q_B^-$, and $Q_AQ_B^{2-}$. In Tables I and II all residues that have van der Waals or electrostatic interaction energies with absolute values larger than 2.0 kcal/mol are listed. Changes in van der Waals energies are generally quite small and will not affect significantly the different bonding affinity of the protein matrix to Q_B. Electrostatic interactions, however, are rather different and mostly more attractive in the case of Q_B^- and Q_B^{2-}.

The strongest interaction of the protein with the neutral ubiquinone is an electrostatic attraction between glutamate L212 and the positively polarized methyl groups and ring system of Q_B. Glutamate L212 has been assumed in our simulation in its anionic form, representing a high-pH situation that is unfavorable for a transfer $Q_A^-Q_B \rightarrow Q_AQ_B^-$. Further dominant interactions have their origin in hydrogen bonding between the carbonyl and ether oxygen atoms of the quinone and the peptide N–H groups of the residues L190 (histidine), L224 (isoleucine), and L225 (glycine) or in electrostatic interaction with L223 (serine) and the positive iron ion.

TABLE I: Interaction of Q_B and Q_B^- with the Protein Matrix[a]

residue		interaction with Q_B, kcal/mol			
		before transfer		after transfer	
type	name	electrostatic	van der Waals	electrostatic	van der Waals
TRP	M23	0.151	−4.318	0.113	−3.996
TYR	M50	0.015	−4.476	0.414	−4.372
TRP	M127	0.111	−4.660	0.190	−5.189
ARG	M130	−1.511	−5.389	−1.687	−5.503
VAL	M131	−0.118	−2.567	−0.112	−2.976
ARG	M134	−0.327	−2.090	−0.208	−2.826
GLU	M232	0.686	−0.043	5.631	−0.320
LEU	L189	−0.035	−3.243	−0.723	−3.462
HIS	L190	−4.853	−3.023	−16.071	−3.040
LEU	L193	0.579	−2.350	−3.843	−2.795
GLU	L212	−17.394	−2.680	6.679	−3.080
GLN	L214	0.506	−3.196	−0.831	−3.616
PHE	L216	0.031	−8.219	−1.800	−8.132
ARG	L217	0.044	−0.348	−2.298	−0.313
VAL	L219	−0.113	−3.228	0.176	−3.790
VAL	L220	−0.442	−3.201	−0.170	−2.687
TYR	L222	1.017	−2.483	0.718	−2.265
SER	L223	−4.562	−2.438	−11.313	−2.642
ILE	L224	−7.842	−5.383	−15.397	−4.605
GLY	L225	−1.926	−2.617	−7.117	−1.988
SER	L228	−2.456	−0.484	−6.535	−0.524
ILE	L229	−1.610	−4.269	−6.313	−4.542
GLU	H177	1.536	−0.249	6.255	−0.322
Fe1		−2.715		−20.724	

[a] Only residues showing an electrostatic or van der Waals interaction in either the Q_B or Q_B^- state with an absolute value of the interaction energy larger than 2.0 kcal/mol are given.

TABLE II: Interaction of Q_B in the States $Q_A^-Q_B^-$ and $Q_AQ_B^{2-}$ with the Protein Matrix[a]

residue		interaction with Q_B, kcal/mol			
		state $Q_A^-Q_B^-$		state $Q_AQ_B^{2-}$	
type	name	electrostatic	van der Waals	electrostatic	van der Waals
TRP	M23	0.162	−3.618	0.143	−4.450
ASP	M27	−2.531	−1.504	−2.248	−2.235
TYR	M50	0.523	−4.541	0.477	−3.694
TRP	M127	0.051	−4.475	0.244	−5.293
ARG	M130	−1.600	−5.163	−1.767	−4.900
VAL	M131	−0.126	−2.973	−0.133	−2.889
ARG	M134	−0.249	−2.026	−0.343	−2.117
ILE	M144	0.081	−2.049	0.032	−2.059
ASP	M230	2.003	−0.096	5.582	−0.198
GLU	M232	6.426	−0.319	36.372	−1.867
ALA	L186	3.305	−0.739	5.515	−0.733
LEU	L189	0.058	−3.924	0.674	−3.710
HIS	L190	−14.620	−2.534	−2.804	−3.217
LEU	L193	−5.048	−3.518	−9.189	−3.396
GLU	L212	6.460	−2.959	17.650	−2.168
ASN	L213	−0.352	−1.014	−3.584	−0.776
TYR	L215	−1.042	−3.357	−0.837	−3.302
PHE	L216	−1.961	−8.006	−1.645	−6.533
ARG	L217	−2.361	−0.312	−1.159	−0.234
VAL	L219	0.202	−2.670	0.170	−3.402
VAL	L220	−0.164	−2.358	−0.020	−2.321
TYR	L222	0.638	−2.056	1.274	−1.515
SER	L223	−10.910	−2.595	−8.871	−1.356
ILE	L224	−16.009	−4.581	−15.826	−3.972
GLY	L225	−8.299	−1.668	−26.447	−2.233
ALA	L226	3.212	−2.741	−6.402	−1.017
SER	L228	−6.998	−0.547	−10.875	−0.455
ILE	L229	−6.286	−4.942	−12.007	−3.678
GLU	H177	6.278	−0.342	7.634	−0.259
Fe1		−21.199		−153.738	

[a] Only residues showing an electrostatic or van der Waals interaction in one of the two states with an absolute value of the interaction energy larger than 2.0 kcal/mol are shown.

After the electron transfer, hydrogen bonding between Q_B^- and the residues L190 (histidine), L224 (isoleucine), and L225 (gly-

cine) becomes much stronger as would be expected. The interaction with serine L223 becomes more attractive, too. We can argue, therefore, that this attraction has its origin in an interaction of the positively polarized part of the amino acid and the carbonyl oxygen atoms of the quinone which have a much larger negative partial charge in the anionic state. Due to the negative charge on the quinone, the attraction to the iron ion is much stronger as well. All the mentioned interactions lead to a stronger binding of Q_B^- compared to that of the neutral quinone. Only the interaction with the negative glutamate L212 is now repulsive and may lead to some destabilization. It can be argued however, that the pK value of L212 (glutamate) is shifted to a higher value, favoring a protonated, neutral glutamic acid. In that case, attraction of the quinone would be weaker and the repulsion of the Q_B^- would disappear or even change into an attractive force.

Interaction energies of Q_B in the state $Q_A^-Q_B^-$ are very similar to those in $Q_AQ_B^-$. The stronger attraction by the positive iron ion is partially compensated for by a repulsion by the negatively charged glutamate M232. Interaction energies become even more attractive in the state $Q_AQ_B^{2-}$. Attraction by the iron ion is now dominant, and if repulsion by glutamate M232 is taken into account, stabilizing electrostatic interaction by the iron complex is still larger than 100 kcal/mol. Reduction of Q_B to Q_B^{2-} under vacuum would require a considerable amount of energy.[23] In the protein environment as it exists in photosynthetic reaction centers such a process could be favored, however, by a strong stabilization of Q_B^{2-} by the protein matrix.

An interesting feature of methoxy-substituted quinones like ubiquinone in *Rhodopseudomonas viridis* is their ability of tuning the electron affinity by varying the dihedral angle defining the position of the methyl group relative to the aromatic ring plane.[53,54] Variation of this dihedral angle can be affected by vibrational motion and interactions with the protein and leads to a change in the charge distribution of the system, i.e., in the atomic partial charges.

5. Summary

We have investigated in this paper the slowest electron-transfer reaction in the photosynthetic reaction center protein complex, $Q_A^-Q_B \rightarrow Q_AQ_B^-$, in which an electron charge is shifted by almost 20 Å. The time scale of the reaction, micro- to milliseconds, does not permit a simulation, but rather we studied structural and dynamical properties before and after the transfer, the response of the protein environment to an enforced transfer (relaxation time and energy change), and the coupling of the transfer to classical protein motion and its influence on the tuning of redox energies of Q_A and Q_B. We also studied in detail the interactions of the reaction intermediates Q_B, Q_B^-, and Q_B^{2-} with the binding site.

Likely the most important aspect of our investigation is the conceptual framework that we have provided for the analysis of molecular dynamics calculations in terms of properties relevant for electron-transfer reactions. Not surprisingly—since molecular dynamics allows only a description of classical motion—the framework is very close to the Marcus theory which deals with the coupling of low-frequency, i.e., classical, solvent motion to electron transfer. However, rather than assuming that the Marcus description necessarily holds, we have shown using classical line-shape functions following Hopfield's treatment[33] that the energy for virtual electron transfer $\Delta E(t)$ in a protein matches perfectly the mold of the Marcus theory with the advantage that one has complete control over all aspects of the theory, i.e., all quantities entering the description can be obtained from simulations and, therefore, can be well understood. The most surprising aspect of our analysis may be that the so-called solvent coordinate appears in the theory only in a very formal way, to describe the distribution of $\Delta E(t)$ values, but is eliminated when actual properties such as electron transfer rates are described. We find it very pleasing that the phenomenon of electron transfer in this context reproduces very nicely the fluctuation–dissipation theorem of nonequilibrium statistical mechanics in that the relaxation time of the correlation function $C_{\Delta E\Delta E}(t)$ is identical with the solvent relaxation time after the transfer, described by the response function $R_{\Delta E\partial/\partial\Delta E}(t)$. The description presented allows one also to express the factor of the electron-transfer rate controlled by coupling to the classical degrees of freedom in terms of a Kubo line-shape function that governs the coupling between fluctuations of $\Delta E(t)$ and a quantum mechanical process. We hope that we have provided a consistent and useful framework, well founded in the previous theories, within which the coupling of classical degrees of freedom to quantum mechanical electron transfer can be analyzed by molecular dynamics simulations.

We may finally comment on our findings regarding the interaction of Q_B in the states $Q_A^-Q_B$, $Q_AQ_B^-$, $Q_A^-Q_B^-$, and $Q_AQ_B^{2-}$ with the protein matrix. These quinone states show different binding strengths which are mainly due to electrostatic interactions with amino acids and the non-heme iron at the binding site. The investigations need, however, to be further improved by accounting for exact atomic charges and for polarization effects.

Acknowledgment. K.S. thanks A. Weller for numerous long and enjoyable discussions regarding the nature of the coupling between electron transfer and solvent motion. The question discussed remained on his minds until he saw a chance with this work to finally address them. We thank J. Deisenhofer for kindly providing us with the X-ray structure of *Rhodopseudomonas viridis* and A. Brünger for making upgraded versions of the program XPLOR available to us. Discussions with H. Treutlein and C. A. Wraight were very helpful and stimulating. M.N. gratefully acknowledges financial support by the Kanton Zürich, Switzerland. The research was carried out in the Center for Parallel Computation in Molecular Dynamics funded by the National Institute of Health. Computing time was granted by the National Center of Supercomputer Applications supported by the National Science Foundation.

(53) Prince, R. C.; Halbert, T. R.; Upton, T. H. In *Advances in Membrane Biochemistry and Bioenergetics*; Kim, C. H., Tedeschi, H., Diwan, J. J., Salerno, J. C., Eds.; Plenum Press: New York, 1988.

(54) Robinson, H. H.; Kahn, S. D. *J. Am. Chem. Soc.*, submitted for publication.

(55) Bash, P. A.; Field, M. J.; Karplus, M. *J. Am. Chem. Soc.* **1989**, *109*, 8092.